Title

Protonation Heterogeneity Modulates the Ultrafast Photocycle Initiation Dynamics of Phytochrome Cph1

Journal

The Journal of Physical Chemistry Letters, 9(12)

ISSN

1948-7185

Authors

Kirpich, Julia S
Mix, L Tyler
Martin, Shelley S
et al.

Publication Date

2018-06-21

DOI

10.1021/acs.jpclett.8b01133

Peer reviewed

HHS Public Access

Author manuscript

J Phys Chem Lett. Author manuscript; available in PMC 2019 June 21.

Published in final edited form as:

J Phys Chem Lett. 2018 June 21; 9(12): 3454–3462. doi:10.1021/acs.jpclett.8b01133.

Protonation Heterogeneity Modulates the Ultrafast Photocycle Initiation Dynamics of Phytochrome Cph1

Julia S. Kirpich[1], **L. Tyler Mix**[1], **Shelley S. Martin**[2], **Nathan C. Rockwell**[2], **J. Clark Lagarias**[2], and **Delmar S. Larsen**[1,*]

[1]Department of Chemistry, University of California, Davis, One Shields Ave, Davis, 95616

[2]Department of Molecular and Cell Biology, University of California, Davis, One Shields Ave, Davis, CA, 95616

Abstract

Phytochromes proteins utilize ultrafast photoisomerization of a linear tetrapyrrole chromophore to detect the ratio of red to far-red light. Femtosecond photodynamics in the PAS-GAF-PHY photosensory core of the Cph1 phytochrome from *Synechocystis* sp. PCC6803 (Cph1Δ) were resolved with a dual-excitation-wavelength-interleaved pump-probe (DEWI) approach with two excitation wavelengths (600 nm and 660 nm) at three pH values (6.5, 8.0, and 9.0). Observed spectral and kinetic heterogeneity in the excited-state dynamics were described with a self-consistent model comprised of three spectrally distinct populations with different protonation states (P_r-I, P_r-II, and P_r-III), each composed of multiple kinetically distinct sub-populations. Apparent partitioning among these populations is dictated by pH, temperature, and excitation wavelength, Our studies provide insight into photocycle initiation dynamics at physiological temperatures, implicate the low-pH/low temperature P_r-I state as the photoactive state *in vitro*, and implicate an internal hydrogen-bonding network in regulating photochemical quantum yield.

Graphical Abstract

*Corresponding Author: Delmar S. Larsen, Department of Chemistry, University of California, Davis, Davis CA 95616. Telephone: (530) 754-9075; dlarsen@ucdavis.edu.

Supporting Information

The Supporting Information (SI) includes the description of the sample preparation, transient absorption experiment and global analysis, table indicating occupancies of the population for the integrated model, comparison of the selected spectra and kinetics at different excitation wavelength and different pH, comparison of SADS and kinetics for different temperatures and excitation wavelength, P_r-I and P_r-II structures. The SI can be found online at: http://pubs.acs.org.

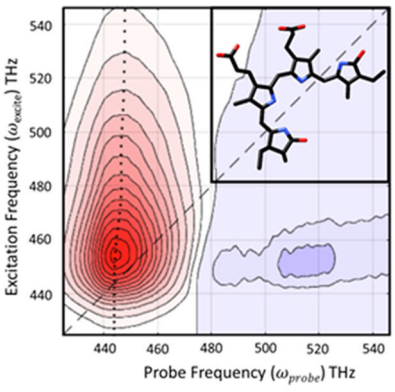

Emerging genetically encoded biological materials allow researchers to control biological activity with light at the cellular or sub-cellular level.[1–7] A common approach in developing such optogenetic materials involves fusing existing light-sensing domains to non-native output domains (e.g., histidine kinase domains or DNA binding proteins) to make novel hybrid photoreceptors. A detailed understanding of the mechanisms that couple light to biological function in existing photoreceptor proteins aids in the engineering of these optogenetic tools. Of the known photoreceptor families, bilin-binding proteins such as phytochromes have attracted interest for such efforts because of their response to long wavelengths that penetrate deeper into mammalian tissue.[8]

Phytochromes are widespread photoreceptors using covalently attached linear tetrapyrrole (bilin) chromophores to switch between red-absorbing P_r and far-red absorbing P_{fr} states (Fig. 1A–B).[9–12] The N-terminal PAS-GAF-PHY photosensory core module of full-length Cph1 (amino acids 1–514, hereafter termed Cph1Δ) from the cyanobacterium *Synechocystis* sp. PCC6803 is one of the most well studied model systems for exploring phytochrome photodynamics due to its robust recombinant expression and known crystal structure (Fig. 1C).[13–15] Full-length Cph1 includes a C-terminal histidine kinase domain, but Cph1 and Cph1Δ exhibit nearly identical fluorescence spectra, activation barriers for the Pr photoreaction, and photodynamics.[16] Red illumination of the dark-adapted P_r state of Cph1Δ (Fig. 1B; red curve) initiates forward photoconversion of the phycocyanobilin (PCB) chromophore (Fig. 1A) to generate the isomerized Lumi-R primary photoproduct on a picosecond timescale.[17–22] Lumi-R evolves on the electronic ground-state surface via several intermediates to generate P_{fr} (Fig. 1B; dark red curve) on a >100 ms timescale.[23, 24] The dark-adapted P_r state is then regenerated from P_{fr} either by far-red light (~700 nm) or via thermal reversion (>24 h).[9, 13, 25]

Under physiological conditions, most proteins continually flex, rotate and sample different metastable states on a complex multi-dimensional potential energy surface.[26, 27] For phytochromes, as for photoreceptors in general, these dynamics result in multiple co-existing populations that often exhibit distinct spectra (“spectral heterogeneity”) and/or distinct kinetics (“temporal heterogeneity”). Both types of heterogeneity reflect structural differences in the chromophore itself, such as in protonation state or facial disposition of the

bilin rings,[28] and/or in the surrounding protein scaffold, such as sidechain conformation[29] or protonation state.[30]

Through analysis of the temperature dependence and excitation wavelength dependence of Cph1Δ fluorescence, Sineshchekov and coworkers provided evidence for the presence of multiple co-existing P_r populations.[16] Using variants of Cph1Δ incorporating specific mutations, they argued that photochemical quantum yield correlates with differences in the relative activation barriers for bifurcating processes on the excited state surface or for partitioning between different sub-populations with different photoactivities.[31, 32] This interpretation assumes that the P_r ground state is spectrally homogenous in solution.[33] However, Matysik and co-workers used magic angle NMR measurements of Cph1Δ at 243 K and pH 8 to resolve two co-existing P_r populations (P_r-I and P_r-II) with different hydrogen bonding networks around the embedded PCB chromophore.[23] Heyne and co-workers similarly argued for inhomogeneity in Cph1 based on polarized transient infrared signals.[34] This work demonstrated the existence of structural heterogeneity in the P_r ground state (i.e., without illumination).

Spectral heterogeneity has also been observed in wild-type Cph1 by examining the wavelength and temperature dependence of static and ultrafast transient absorption (TA) signals for Cph1Δ at pH 8, revealing two co-existing P_r populations denoted $^{photo}P_r$ and $^{fluor}P_r$.[35] Excitation of each of these populations yielded multiple spectrally identical excited-state P_r* sub-populations that decayed on different timescales (temporal heterogeneity), with P_r* sub-populations arising from $^{photo}P_r$ excitation being spectrally distinct from those arising from $^{fluor}P_r$ excitation. The fluorescence excitation spectrum of Cph1Δ corresponds well with the extracted $^{fluor}P_r$ static spectrum, so the room-temperature fluorescence spectrum of Cph1Δ was assigned to this species.[35] This interpretation led to the conclusion that only one $^{photo}P_r$ sub-population was almost exclusively responsible for generation of the Lumi-R primary photoproduct. Remarkably, this ground state heterogeneity is dependent on a temperature-dependent dynamic equilibrium: the longer-living $^{fluor}P_r$ population is favored at elevated temperatures, resulting in inverted Ârrhenius behavior for photochemistry.[35] Such behavior is difficult to reconcile with a single homogeneous P_r ground state.

Further support for a heterogeneous P_r ground state was obtained in a recent study of the pH dependence of the static absorption and resonance Raman spectra of Cph1Δ,[36] which identified three populations with differing pH-dependent amplitudes that were ascribed to different intra-protein hydrogen-bonding networks:

- P_r-I that dominates at low pH values (<pH 7)
- P_r-II that has its greatest amplitude at ~pH 8.5
- Pr_{dep} that dominates at higher pH values.

Despite this robust evidence for ground state heterogeneity in the P_r state of Cph1Δ, other studies continue to use homogeneous models for data analysis. However, ignoring ground state heterogeneity would lead to incorrect conclusions about Cph1Δ's underlying ultrafast dynamics. For example, a homogeneous model was used to interpret the femtosecond

stimulated Raman signals of Cph1Δ at pH 8, leading to the proposal that isomerization occurs exclusively on the excited-state surface.[22] Subsequent broadband pump-dump-probe spectroscopic signals revealed this to be an erroneous conclusion.[37] Similarly, 2-dimensional (2D) TA spectroscopy was recently used to conclude that Cph1Δ is homogeneous at 298 K and pH 8.[38].

The present study was undertaken to reexamine heterogeneity of the P_r ground state of Cph1Δ in light of the reported 2D results. We consider the following questions: If Cph1Δ is heterogeneous, why do 2D signals[38] support a homogeneous P_r model? What is the basis of the temperature-dependent heterogeneity observed by Kim et al.[35] and the pH dependent heterogeneity observed by Escobar et al.?[36] What consequences does this heterogeneity have for the functional photoactivity of Cph1Δ? To address these questions, we characterized the excitation-wavelength dependence of ultrafast TA signals at three pHs (6.5, 8.0, and 9.0). To minimize differences in setup between datasets, we used Dual-Excitation-Wavelength-Interleaved Transient Absorption (DEWI)[39–41] to collect two alternating broadband TA signals near simultaneously (within 4 ms) on a single sample (here, a single pH value) while maintaining all other experimental conditions unchanged. This protocol removes errors caused by long-term fluctuations of excitation power, sample degradation, and different experimental conditions. As such, DEWI TA measurements represent a powerful approach to interrogate the photo-induced kinetics of underlying ground state populations with different absorption properties. Based on these measurements, we have been able to re-interpret the temperature dependent TA and static absorption signals from Kim et al.[35] to construct a self-consistent, heterogeneous global model describing the photoinitiation dynamics of Cph1Δ that is in strong agreement with the pH dependent vibrational signals from Escobar et al[36] and that can simulate the reported 2D TA spectroscopy results.[38]

We began by examining the static absorption of our preparation of Cph1Δ as a function of pH. In agreement with previous reports,[24, 36] the dark-adapted (P_r) absorption spectrum of Cph1Δ was pH dependent (Fig. 2). At pH 6.5, the absorption spectrum peaked at 664 nm (Fig. 2, dark red curves) with a high-energy shoulder at 610 nm. At pH 8.0, the spectrum blue-shifted slightly to 662 nm (orange curves), exhibiting a slight increase of the high-energy shoulder. The spectrum changed significantly at pH 9.0 (blue curves), with a more prominent shoulder and a further blue shift to 650 nm. These data thus can be interpreted as arising from at least two species, with one or more blue-shifted populations becoming more important contributors to the observed spectrum at high pH. This interpretation can also be applied to previous studies of pH[24, 36] and temperature dependence.[33, 35] Hence, it is possible that the same underlying heterogeneity of Cph1Δ in the P_r state can be resolved in both temperature-dependent and pH-dependent spectra. We therefore used DEWI measurements at different pH values to provide a comparison to our previous use of the DEWI technique at different temperatures.[35]

Selected DEWI TA spectra and kinetics of Cph1Δ at three pHs (6.5, 8.0, and 9.0) are contrasted in Figs. 3 and S1–S4. These measurements reveal a strong excitation-wavelength and pH dependence of the primary photodynamics. At pH 8, the most common pH used for ultrafast studies, the 660-nm excitation TA spectrum at 1 ps (Fig. 3B; red curve) exhibited a pronounced negative band around 675 nm, attributed to overlapping ground-state bleach

(GSB) and simulated emission (SE) bands, with a broad positive excited-state absorption (ESA) band from 450 nm to 625 nm.[35] The 600-nm excitation TA spectrum (blue curve) exhibited similar features but had a slightly blue-shifted (10 nm) GSB/SE band and a significantly weaker ESA from 550–625 nm. The raw spectra resembled the previously described $^{photo}P_r$* (660 nm excitation) and $^{fluor}P_r$* (600 nm excitation) populations.[35] These results show that this preparation behaves similarly to that used in the previous DEWI study and confirms that at least two populations co-exist at pH 8. The $^{fluor}P_r$* population is longer lived than $^{photo}P_r$*, consistent with initiation of the Cph1 photocycle via one or more members of the $^{photo}P_r$* sub-population ensemble (Fig. S5).

Differences between excitation wavelengths were less pronounced at pH 6.5. The 660-nm excitation spectrum (Fig. 3A; red curve) strongly resembled the $^{photo}P_r$* spectrum observed at pH 8 (Fig. 3B; red curve). The 600-nm spectrum at pH 6.5 (Fig. 3A; blue curve) also resembled $^{photo}P_r$*, although with a weaker amplitude $^{fluor}P_r$* population. This behavior is also reflected in the kinetics (Figs. S3 and S4). Hence, while the $^{photo}P_r$*/ $^{fluor}P_r$* heterogeneity observed at pH 8.0 also exists at pH 6.5, lower pH skewed the P_r population ensemble toward $^{photo}P_r$*. In contrast, the pH 9.0 signals exhibited a more pronounced excitation-wavelength dependence. The 1-ps spectrum after 660 nm excitation at pH 9.0 (Fig. 3C; red curve) was more similar to that observed for 600 nm than that observed for 660 nm at pH 8.0 (Fig. 3B; blue and red curves, respectively). The 600-nm excitation spectrum at pH 9.0 (Fig. 3C; blue curve) exhibited a strong negative GSB at 600 nm that overlaps the GSB/SE band already attributed to $^{photo}P_r$*. Hence, the heterogeneity observed at pH 9 clearly differs from that at pH 6.5 and 8.0 and may include a new ‘deprotonated’ population that was preferentially excited at 600 nm. Consistent with this interpretation, this new population also exhibited longer living kinetics than both $^{fluor}P_r$* and $^{photo}P_r$* (Fig. S4A).

The DEWI data qualitatively support the hypothesis that the pH-dependent and temperature-dependent signals reflect underlying heterogeneity arising from three spectrally distinct ground state populations, as proposed.[36] We can thus combine the nomenclature from this work and from the previous DEWI study,[35] as follows:

- P_r-I is $^{photo}P_r$,
- P_r-II is $^{fluor}P_r$, and
- P_r-III is the new population observed at high pH with a deprotonated PCB chromophore (previously called Pr_{dep}).[36]

It is important to note that the P_r-III population is not red-absorbing; rather, it exhibits a green-yellow GSB resembling that observed for the green-absorbing *15Z* state of cyanobacteriochrome (CBCR) RcaE.[41] Chromophore deprotonation is known to cause a green-yellow absorption of free PCB extracted from *Synechocystis sp.* PCC 6803,[42] green absorption in RcaE[30] and is thought to cause similar peak absorption in variants of another CBCR.[29] However, we have chosen to retain the designation Pr-III in the current work for simplicity.[36] Applying this nomenclature to our data, the P_r sample at pH 9.0 consists primarily of P_r-II and P_r-III populations, whereas the pH 8 sample consisted primarily of P_r-I, with some P_r-II, and the pH 6.5 sample was almost exclusively P_r-I.

We previously employed multi-wavelength global analysis to develop a framework for interpreting temperature-dependent DEWI.[35] This model successfully described data taken at pH 8, but it seemed likely that it would be insufficient at pH 9 because of the possible presence of P_r-III. We therefore extended this model to evaluate the six DEWI TA datasets from Fig. 3, with the goal of having a single, self-consistent model to describe the ultrafast photodynamics of multiple ground state populations as a function of pH, temperature, and excitation wavelength.

The proposed model includes three spectrally distinct populations (color boxes in Fig. 4), each of which is an ensemble of multiple temporally-distinct sub-populations (e.g., P_r-Ia*). The three ground state populations are in a dynamic equilibrium that is sensitive to both pH and temperature. We estimate that initial Franck-Condon cooling occurs after excitation with a 120-fs time constant, but current data do not allow us to resolve differences in Franck-Condon dynamics between the sub-populations. The three populations then give rise to three spectrally distinct relaxed excited-state populations, each of which decays as two (P_r-I and P_r-III) or three (P_r-II) spectrally identical but temporally distinct sub-populations.

Global analysis was used to extract the characteristic species-associated difference spectra (SADS, Fig. 5) from this target model for P_r-I* (teal curve), fluorescent P_r-II* (green curve), and deprotonated P_r-III* (purple curve). The SADS were in good agreement with the raw DEWI TA data in Fig. 3 and the temperature dependent DEWI data of Kim et al. (Fig. S6).[35] Moreover, this model accurately described the observed multiphasic kinetics as a function of pH and excitation wavelength (Figs. S3 and S4) as well as describing kinetics as a function of temperature (Fig. S7).[35] Therefore, we conclude that a single model can describe the observed heterogeneity of Cph1Δ in the P_r state under these different conditions. However, this model would also need to describe the apparent homogeneity of Cph1Δ P_r in 2D spectroscopy.[38] In multi-chromophore systems with strongly congested spectral features like photosynthetic complexes,[43] fully resolved 2D signals allow tracking the dynamics of all spectrally distinct populations. This approach can suffer from Fourier transform artifacts such as phasing, but this does not seem to be the case for 2D study of Cph1Δ.[38] We therefore tested whether “apparent” homogeneous 2D data of Cph1Δ (measured at pH 8 and room temperature) can be simulated using the heterogeneous model presented in Figs. 4 and 5. The 9-ps 2D spectrum was calculated using a simple kinetic approach (see Supporting Information) from the spectral and kinetic responses for the induced dynamics under these conditions (Fig. 4). The response for each state ($R_{Pr\text{-}I}$, $R_{Pr\text{-}II}$ and $R_{Pr\text{-}III}$ for P_r-I, P_r-II and P_r-III states, respectively) is expanded in terms of constituent dynamics of the sub-populations (e.g. P_r-Ia and P_r-IIb for the P_r-I state):

$$R_{Pr}\left(t, \omega_{probe}\right) = \sum_{i=1}^{n} c_i(t)\, \Delta\, \varepsilon_i\left(\omega_{probe}\right)$$

where i correspond to the relevant transient species in each of the three states (e.g. $^{FC}P_r$-Ia, P_r-Ia, $^{FC}P_r$-IIb, P_r-IIb and Lumi-R for the P_r-I state), $\Delta\, \varepsilon_i$ are the estimated SADS (Fig. 5), $c_i(t)$ are the associated concentration profiles for each transient population and t is the time between excitation and probe pulses at is set to 9 ps for the simulation in Figure 6. These

responses for the three states are then individually scaled by the associated absorption spectra $\sigma(\omega_{excite})$ for each state, estimated from temperature dependent analysis,[35] to simulate the 2D spectra:

$$2D(\omega_{excite}, t, \omega_{probe}) = B(\omega_{excite}, \omega_{probe})\left[\sigma_{P_r-I}(\omega_{excite}) R_{P_r-I}(t, \omega_{probe}) + \sigma_{P_r-II}(\omega_{excite}) R_{P_r-II}(t, \omega_{probe}) + \sigma_{P_r-III}(\omega_{excite}) R_{P_r-III}(t, \omega_{probe})\right]$$

where $B(\omega_{excite}, \omega_{probe})$ is a bandwidth factor to match the spectral response of the 2D experiment (not needed for TA signals) that is modeled by a 2D Gaussian with 200-nm Full Width at Half Maximum for this to matched the bandwidth of the experiment.[38] R_{P_r-III} was not included in the simulation because the P_r-III population is negligibly populated at pH 8 and room temperature.

Remarkably, the simulated 9-ps 2D spectrum strongly resembles the published experimental spectrum (Fig. 6).[38] In particular, the GSB/SE band (red peak) is off the diagonal and exhibits an elongation along the excitation frequency axis. Elongation of the spectra along the diagonal is considered a key hallmark of heterogeneity in 2D spectra (diagonal shown in Fig. 6 as a purple line);[44] indeed, its absence in the experimental 2D data is a key part of the rationale advanced for a homogeneous Cph1Δ P_r state.[38] However, the heterogeneity observed in the DEWI-TA signals is observed in the simulated 2D spectra as a slight shift in the observed peak emission frequency as a function of excitation frequency and as a shifting peak of the signal (sliced along the probe frequency) as function of excitation frequency. This peak shifts from ~425 THz at low-energy excitation frequencies (i.e., red wavelengths) where P_r-I is preferentially excited (Fig. 6, teal curves) to 447 THz at high-energy excitation frequencies (i.e., blue wavelengths) where P_r-II is preferentially excited (green curves). The same trend can be seen in the published experimental 9 ps spectrum.[38] The expected "elongation" is actually a shift in peak emission frequency as the excitation frequency changes, and that behavior is present in Cph1Δ. The frequency shift does not strictly follow the diagonal in Cph1Δ, because it is not continuous variation; instead, there is a discrete transition between P_r-I and P_r-II as the excitation wavelength changes. The 2D data do not demonstrate that Cph1Δ is homogeneous, but rather provide a high-quality demonstration that the underlying heterogeneity is not continuous.

The heterogeneity of the three populations, P_r-I, P_r-II, and P_r-III, arises on the ground-state surface, because these populations can be distinguished by changes in static absorbance spectroscopy and in the GSB bands in TA spectroscopy as their relative occupancies vary with changing pH and temperature. Each of these populations is composed of two to three spectrally identical sub-populations that evolve with different time constants. The structural basis for these kinetically distinct sub-populations is less clear: they may also arise from ground-state heterogeneity, or they may arise due to bifurcation on the excited-state surface. For example, it is possible that the presence of alternate side-chain rotamers for an aliphatic residue near the chromophore would not result in spectral differences but would result in different steric clashes as the chromophore undergoes photoisomerization. In this case,

ground state heterogeneity would manifest in kinetically distinct but spectrally identical sub-populations. However, it is also possible that there are multiple pathways for structural evolution of the chromophore during photoisomerization that need not produce detectably large spectral shifts, such as different directions for rotation of the D-ring.[45]

The protein-chromophore hydrogen bonding network in Cph1 involves the PCB chromophore, bound water molecules, and multiple protein residues (Fig. 7).[15] The conserved His260 is proposed to be a key residue in this network: vibrational spectroscopy implicates differences in the protonation state of His260 in the differences between P_r-I and P_r-II,[36] and a combination of spectroscopic techniques and theoretical modeling has allowed proposal of structural models for the two species (Fig. 7).[46, 47] However, the equilibrium between P_r-I and P_r-II is accompanied by a significant change in heat capacity (ΔC_p = 446 ± 53 cal mol^{-1} K^{-1}).[35] It thus seems plausible that structural differences between these populations propagate beyond the immediate milieu of the chromophore.

Our data support the conclusion that the low-temperature/low pH P_r-I state is the photoactive state *in vitro*. Based on Resonance Raman and solid-state NMR spectroscopy, the P_r-I state possesses a cationic His260 that is H-bonded directly to the C-ring propionate and held orthogonal to the positively charged chromophore (Fig. 7A). If the low-temperature/low-pH state is photochemically active, it follows that the blue-shifted higher-temperature/higher-pH P_r-II state can be assigned to the photoinactive, fluorescent population. Relative to P_r-I, P_r-II is thought to possess an altered hydrogen-bonding network with a bridging water that lies between the neutral imidazole sidechain of His260 and the C-ring propionate and hence would match the interactions seen in the crystal structure (Fig. 7B). In this regard, it is interesting to note that crystals used to determine the Cph1 structure[46] were grown at 18°C (favoring P_r-I) and slightly acidic pH (favoring P_r-II),[15] so it seems plausible that either state (or both) could be present.

Finally, P_r-III possesses a deprotonated PCB chromophore with an unresolved hydrogen-bonding network. No photoproduct from this population was observed in the DEWI TA data, and it exhibits an even longer excited-state lifetime than P_r-II (Fig. 4). We therefore propose that P_r-III is even less active than P_r-II. The P_r-III state is not appreciably occupied at pH≤8. Significant pH fluctuations can occur transiently under high light illumination of cyanobacteria, leading to the idea that the CBCRs controlling complementary chromatic acclimation like RcaE are regulated by both light and pH.[30] The photosensory function of Cph1 may be similarly modulated when light fluence rates are high.

Our work is consistent with a critical role for His260 in dictating effective photochemical quantum yields in phytochromes. His260 is highly conserved in phytochromes and lies within 3.0 Å of the PCB chromophore (Figs. S8 and S9). Given the positive charge on the PCB chromophore, the protonated His260 sidechain in P_r-I would be expected to adopt a conformation that minimizes electrostatic repulsion of the two cationic moieties. It has been proposed that a charged Arg residue in PYP is responsible for shifting the excited-state surface to direct the excited state toward an isomerization coordinate and away from non-productive quenching coordinates (single bond rotations).[48] However, the H260Q mutant of

Cph1Δ exhibits static spectral features of the P_r-I state and still photoconverts to P_{fr},[42] so the positive charge of protonated His260 is not essential for photoconversion in phytochromes.

Understanding the molecular basis for this dynamic heterogeneity also holds great potential for the rational design of efficient phytochrome-based fluorescent probes. The spectral and kinetic behavior of P_r-II strongly resemble those of the photochemically compromised and highly fluorescent Y176H variant of Cph1Δ, suggesting both cases use similar mechanisms for reduced photochemical quantum yield.[35, 49] It was originally proposed that the Y176H substitution resulted in increased steric hindrance to photoisomerization of the PCB D-ring, [49] but this hypothesis predates the availability of phytochrome crystal structures. It now seems plausible that this substitution disrupts the hydrogen bonding network of the P_r-I population (Fig. 7A). Hydrogen bonding effects are similarly thought to be critical in modulating the excited-state dynamics of the SaBphP1 bacteriophytochrome from *Stigmatella aurantiaca*, in which excited-state proton transfer is thought to be responsible for lowering both the fluorescence and photochemical quantum yields for the biliverdin chromophores of this photoreceptor family.[50, 51]

To conclude, in Cph1Δ, heterogeneity strongly affects kinetics, absorption, fluorescence, and quantum yields (both photochemical and fluorescent), with evidence implicating structural rearrangements and possibly even effects on *in vivo* function. Excitation-wavelength dependent and pH-dependent transient absorption measurements were used to reconcile spectral heterogeneity observed in static absorption and resonance Raman measurements with that observed in temperature-dependent and excitation-wavelength-dependent absorption and transient spectra in Cph1Δ. We ascribe this heterogeneity to heterogeneous protonation of either the bilin chromophore or residues within its immediate environment. We observe three spectrally distinct populations, each having multiple sub-populations distinguished by differing excited-state quenching kinetics. We used a single global model to describe how excitation wavelength, temperature, and pH affect the photocycle initiation dynamics of Cph1Δ. This model also successfully simulated reported 2D electronic spectra, [38] demonstrating that existing approaches for interpreting heterogeneity in such spectra can be misleading. Given the conservation of His260 in most phytochromes, it seems likely that similar effects are widespread in this photoreceptor family.

Supplementary Material

Refer to Web version on PubMed Central for supplementary material.

ACKNOWLEDGEMENTS

This work was supported by grants from the Chemical Sciences, Geosciences, and Biosciences Division, Office of Basic Energy Sciences, Office of Science, United States Department of Energy (DOE DE-FG02–09ER16117) to both J.C.L. and D.S.L., and from the NIGMS-NIH (GM068552) and the USDA National Institute of Food and Agriculture, Hatch project number CA-D*-MCB-4126-H to J.C.L. The authors also thank Chen Song and Jörg Matysik (University of Leipzig) for graciously providing the model coordinates for the P_r-I structure and Jon Hughes (University of Giessen), Vitaly Sineshchekov (Moscow State University), and Francisco Escobar (Technical University Berlin) are thanks for critical discussions. Dr. Mikas Vengris (Light Conversion Ltd.) is acknowledged for the donation of global and target analysis software.

REFERENCES

[1]. Möglich A, and Moffat K (2010) Engineered photoreceptors as novel optogenetic tools, Photochem. Photobiol. Sci 9, 1286–1300. [PubMed: 20835487]

[2]. Shcherbakova DM, Shemetov AA, Kaberniuk AA, and Verkhusha VV (2015) Natural Photoreceptors as a Source of Fluorescent Proteins, Biosensors, and Optogenetic Tools, Annual Review of Biochemistry 84, 519–550.

[3]. Endo M, and Ozawa T (2017) Strategies for development of optogenetic systems and their applications, Journal of Photochemistry and Photobiology C: Photochemistry Reviews 30, 10–23.

[4]. Di Ventura B, and Kuhlman B (2016) Go in! Go out! Inducible control of nuclear localization, Current Opinion in Chemical Biology 34, 62–71. [PubMed: 27372352]

[5]. Beyer HM, Juillot S, Herbst K, Samodelov SL, Müller K, Schamel WW, Römer W, Schäfer E, Nagy F, Strähle U, Weber W, and Zurbriggen MD (2015) Red Light-Regulated Reversible Nuclear Localization of Proteins in Mammalian Cells and Zebrafish, ACS Synthetic Biology 4, 951–958. [PubMed: 25803699]

[6]. Spiltoir JI, Strickland D, Glotzer M, and Tucker CL (2016) Optical Control of Peroxisomal Trafficking, ACS Synthetic Biology 5, 554–560. [PubMed: 26513473]

[7]. Wu YI, Frey D, Lungu OI, Jaehrig A, Schlichting I, Kuhlman B, and Hahn KM (2009) A genetically encoded photoactivatable Rac controls the motility of living cells, Nature 461, 104. [PubMed: 19693014]

[8]. Filonov GS, Piatkevich KD, Ting L-M, Zhang J, Kim K, and Verkhusha VV (2011) Bright and stable near-infrared fluorescent protein for in vivo imaging, Nature Biotechnology 29, 757.

[9]. Rockwell NC, Su YS, and Lagarias JC (2006) Phytochrome structure and signaling mechanisms, Annu Rev Plant Biol 57, 837–858. [PubMed: 16669784]

[10]. Rockwell NC, and Lagarias JC (2010) A brief history of phytochromes, ChemPhysChem 11, 1172–1180. [PubMed: 20155775]

[11]. Burgie ES, and Vierstra RD (2014) Phytochromes: An atomic perspective on photoactivation and signaling, Plant Cell 26, 4568–4583. [PubMed: 25480369]

[12]. Anders K, and Essen L-O (2015) The family of phytochrome-like photoreceptors: diverse, complex and multi-colored, but very useful, Current Opinion in Structural Biology 35, 7–16. [PubMed: 26241319]

[13]. Yeh KC, Wu SH, Murphy JT, and Lagarias JC (1997) A cyanobacterial phytochrome two-component light sensory system, Science 277, 1505–1508. [PubMed: 9278513]

[14]. Remberg A, Lindner I, Lamparter T, Hughes J, Kneip C, Hildebrandt P, Braslavsky SE, Gärtner W, and Schaffner K (1997) Raman Spectroscopic and Light-Induced Kinetic Characterization of a Recombinant Phytochrome of the Cyanobacterium Synechocystis, Biochemistry 36, 13389–13395. [PubMed: 9341232]

[15]. Essen LO, Mailliet J, and Hughes J (2008) The structure of a complete phytochrome sensory module in the Pr ground state, Proc. Natl. Acad. Sci. USA 105, 14709–14714. [PubMed: 18799745]

[16]. Sineshchekov V, Koppel L, Esteban B, Hughes J, and Lamparter T (2002) Fluorescence investigation of the recombinant cyanobacterial phytochrome (Cph1) and its C-terminally truncated monomeric species (Cph1 Delta 2): implication for holoprotein assembly, chromophore-apoprotein interaction and photochemistry, J. Photochem. Photobiol. B 67, 39–50. [PubMed: 12007466]

[17]. Heyne K, Herbst J, Stehlik D, Esteban B, Lamparter T, Hughes J, and Diller R (2002) Ultrafast dynamics of phytochrome from the cyanobacterium Synechocystis, reconstituted with phycocyanobilin and phycoerythrobilin, Biophys. J 82, 1004–1016. [PubMed: 11806940]

[18]. van Thor JJ, Ronayne KL, and Towrie M (2007) Formation of the early photoproduct Lumi-R of cyanobacterial phytochrome Cph1 observed by ultrafast mid-infrared spectroscopy, J. Am. Chem. Soc 129, 126–132. [PubMed: 17199291]

[19]. van Wilderen L, Clark IP, Towrie M, and van Thor JJ (2009) Mid-Infrared Picosecond Pump-Dump-Probe and Pump-Repump-Probe Experiments to Resolve a Ground-State Intermediate in Cyanobacterial Phytochrome Cph1, Journal of Physical Chemistry B 113, 16354–16364.

[20]. Yang Y, Linke M, von Haimberger T, Hahn J, Matute R, Gonzalez L, Schmieder P, and Heyne K (2012) Real-Time Tracking of Phytochrome's Orientational Changes During Pr Photoisomerization, J. Am. Chem. Soc 134, 1408–1411. [PubMed: 22229806]

[21]. Fitzpatrick AE, Lincoln CN, van Wilderen LJ, and van Thor JJ (2012) Pump-dump-probe and pump-repump-probe ultrafast spectroscopy resolves cross section of an early ground state intermediate and stimulated emission in the photoreactions of the Pr ground state of the cyanobacterial phytochrome Cph1, J Phys Chem B 116, 1077–1088. [PubMed: 22098118]

[22]. Dasgupta J, Frontiera RR, Taylor KC, Lagarias JC, and Mathies RA (2009) Ultrafast excited-state isomerization in phytochrome revealed by femtosecond stimulated Raman spectroscopy, Proceedings of the National Academy of Sciences of the United States of America 106, 1784–1789. [PubMed: 19179399]

[23]. Rohmer T, Lang C, Hughes J, Essen LO, Gartner W, and Matysik J (2008) Light-induced chromophore activity and signal transduction in phytochromes observed by C-13 and N-15 magic-angle spinning NMR, Proceedings of the National Academy of Sciences of the United States of America 105, 15229–15234. [PubMed: 18832155]

[24]. van Thor JJ, Borucki B, Crielaard W, Otto H, Lamparter T, Hughes J, Hellingwerf KJ, and Heyn MP (2001) Light-induced proton release and proton uptake reactions in the cyanobacterial phytochrome Cph1, Biochem. (ACS) 40, 11460–11471.

[25]. Rohmer T, Lang C, Bongards C, Gupta K, Neugebauer J, Hughes J, Gartner W, and Matysik J (2010) Phytochrome as Molecular Machine: Revealing Chromophore Action during the Pfr → Pr Photoconversion by Magic-Angle Spinning NMR Spectroscopy (vol 132, pg 4431, 2010), Journal of the American Chemical Society 132, 9219–9219.

[26]. Bu Z, and Callaway DJE (2011) Chapter 5 - Proteins MOVE! Protein dynamics and long-range allostery in cell signaling, In Advances in Protein Chemistry and Structural Biology (Donev R, Ed.), pp 163–221, Academic Press.

[27]. Frauenfelder H, Chen G, Berendzen J, Fenimore PW, Jansson H, McMahon BH, Stroe IR, Swenson J, and Young RD (2009) A unified model of protein dynamics, Proceedings of the National Academy of Sciences 106, 5129–5134.

[28]. Rockwell NC, Duanmu D, Martin SS, Bachy C, Price DC, Bhattacharya D, Worden AZ, and Lagarias JC (2014) Eukaryotic algal phytochromes span the visible spectrum, Proceedings of the National Academy of Sciences 111, 3871–3876.

[29]. Lim S, Yu Q, Gottlieb SM, Chang C-W, Rockwell NC, Martin SS, Madsen D, Lagarias JC, Larsen DS, and Ames JB (2018) Correlating structural and photochemical heterogeneity in cyanobacteriochrome NpR6012g4, Proceedings of the National Academy of Sciences.

[30]. Hirose Y, Rockwell NC, Nishiyama K, Narikawa R, Ukaji Y, Inomata K, Lagarias JC, and Ikeuchi M (2013) Green/red cyanobacteriochromes regulate complementary chromatic acclimation via a protochromic photocycle, Proceedings of the National Academy of Sciences of the United States of America 110, 4974–4979. [PubMed: 23479641]

[31]. Mailliet J, Psakis G, Feilke K, Sineshchekov V, Essen L-O, and Hughes J (2011) Spectroscopy and a High-Resolution Crystal Structure of Tyr263 Mutants of Cyanobacterial Phytochrome Cph1, Journal of Molecular Biology 413, 115–127. [PubMed: 21888915]

[32]. Sineshchekov V, Mailliet J, Psakis G, Feilke K, Kopycki J, Zeidler M, Essen L-O, and Hughes J (2014) Tyrosine 263 in Cyanobacterial Phytochrome Cph1 Optimizes Photochemistry at the prelumi-R→lumi-R Step, Photochemistry and Photobiology 90, 786–795. [PubMed: 24571438]

[33]. Spillane KM, Dasgupta J, Lagarias JC, and Mathies RA (2009) Homogeneity of phytochrome Cph1 vibronic absorption revealed by resonance Raman intensity analysis, J. Am. Chem. Soc 131, 13946–13948. [PubMed: 19739629]

[34]. Yang Y, Linke M, von Haimberger T, Matute R, González L, Schmieder P, and Heyne K (2014) Active and silent chromophore isoforms for phytochrome Pr photoisomerization: An alternative evolutionary strategy to optimize photoreaction quantum yields, Structural Dynamics 1, 014701. [PubMed: 26798771]

[35]. Kim PW, Rockwell NC, Martin SS, Lagarias JC, and Larsen DS (2014) Dynamic inhomogeneity in the photodynamics of cyanobacterial phytochrome Cph1, Biochem. (ACS) 53, 2818–2826.

[36]. Velazquez Escobar F, Lang C, Takiden A, Schneider C, Balke J, Hughes J, Alexiev U, Hildebrandt P, and Mroginski MA (2017) Protonation-Dependent Structural Heterogeneity in the Chromophore Binding Site of Cyanobacterial Phytochrome Cph1, The Journal of Physical Chemistry B 121, 47–57. [PubMed: 27966353]

[37]. Kim PW, Rockwell NC, Freer LH, Chang C-W, Martin SS, Lagarias J., Clark, and Larsen DS (2013) Unraveling the Primary Isomerization Dynamics in the Cph1 Cyanobacterial Phytochrome with Multipulse Manipulations, Journal of Physical Chemistry Letters 4, 2605–2609. [PubMed: 24143267]

[38]. Bizimana LA, Epstein J, Brazard J, and Turner DB (2017) Conformational Homogeneity in the Pr Isomer of Phytochrome Cph1, The Journal of Physical Chemistry B 121, 2622–2630. [PubMed: 28282147]

[39]. Larsen DS, Papagiannakis E, van Stokkum IHM, Vengris M, Kennis JTM, and van Grondelle R (2003) Excited state dynamics of beta-carotene explored with dispersed multi-pulse transient absorption, Chemical Physics Letters 381, 733–742.

[40]. Kim PW, Freer LH, Rockwell NC, Martin SS, Lagarias JC, and Larsen DS (2012) Femtosecond Photodynamics of the Red/Green Cyanobacteriochrome NpR6012g4 from Nostoc punctiforme. 2. Reverse Dynamics, Biochemistry 51, 619–630. [PubMed: 22148731]

[41]. Gottlieb SM, Kim PW, Rockwell NC, Hirose Y, Ikeuchi M, Lagarias JC, and Larsen DS (2013) Primary photodynamics of the green/red-absorbing photoswitching regulator of the chromatic adaptation E domain from Fremyella diplosiphon, Biochem. (ACS) 52, 8198–8208.

[42]. Hahn J, Strauss HM, Landgraf FT, Gimenez HF, Lochnit G, Schmieder P, and Hughes J (2006) Probing protein-chromophore interactions in Cph1 phytochrome by mutagenesis, The FEBS journal 273, 1415–1429. [PubMed: 16689929]

[43]. Thyrhaug E, Žídek K, Dostál J, Bína D, and Zigmantas D (2016) Exciton Structure and Energy Transfer in the Fenna–Matthews–Olson Complex, The Journal of Physical Chemistry Letters 7, 1653–1660. [PubMed: 27082631]

[44]. Tokmakoff A (2000) Two-Dimensional Line Shapes Derived from Coherent Third-Order Nonlinear Spectroscopy, The Journal of Physical Chemistry A 104, 4247–4255.

[45]. Rockwell NC, Shang L, Martin SS, and Lagarias JC (2009) Distinct classes of red/far-red photochemistry within the phytochrome superfamily, Proceedings of the National Academy of Sciences of the United States of America 106, 6123–6127. [PubMed: 19339496]

[46]. Song C, Psakis G, Lang C, Mailliet J, Gartner W, Hughes J, and Matysik J (2011) Two ground state isoforms and a chromophore D-ring photoflip triggering extensive intramolecular changes in a canonical phytochrome, Proceedings of the National Academy of Sciences of the United States of America 108, 3842–3847. [PubMed: 21325055]

[47]. Mroginski MA, von Stetten D, Escobar FV, Strauss HM, Kaminski S, Scheerer P, Gunther M, Murgida DH, Schmieder P, Bongards C, Gartner W, Mailliet J, Hughes J, Essen LO, and Hildebrandt P (2009) Chromophore Structure of Cyanobacterial Phytochrome Cph1 in the Pr State: Reconciling Structural and Spectroscopic Data by QM/MM Calculations, Biophysical Journal 96, 4153–4163. [PubMed: 19450486]

[48]. Groenhof G, Schäfer LV, Boggio-Pasqua M, Grubmüller H, and Robb MA (2008) Arginine52 Controls the Photoisomerization Process in Photoactive Yellow Protein, Journal of the American Chemical Society 130, 3250–3251. [PubMed: 18293978]

[49]. Fischer AJ, and Lagarias JC (2004) Harnessing phytochrome's glowing potential, Proc. Natl. Acad. Sci. USA 101, 17334–17339. [PubMed: 15548612]

[50]. Toh KC, Stojkovic EA, van Stokkum IHM, Moffat K, and Kennis JTM (2010) Proton-transfer and hydrogen-bond interactions determine fluorescence quantum yield and photochemical efficiency of bacteriophytochrome, Proceedings of the National Academy of Sciences of the United States of America 107, 9170–9175. [PubMed: 20435909]

[51]. Mathes T, Ravensbergen J, Kloz M, Gleichmann T, Gallagher KD, Woitowich NC, St. Peter R, Kovaleva SE, Stojković EA, and Kennis JTM (2015) Femto- to Microsecond Photodynamics of an Unusual Bacteriophytochrome, The Journal of Physical Chemistry Letters 6, 239–243. [PubMed: 26263456]

[52]. Kim PW, Rockwell NC, Martin SS, Lagarias JC, and Larsen DS (2014) Heterogeneous Photodynamics of the Pfr State in the Cyanobacterial Phytochrome Cph1, Biochemistry 53, 4601–4611. [PubMed: 24940993]

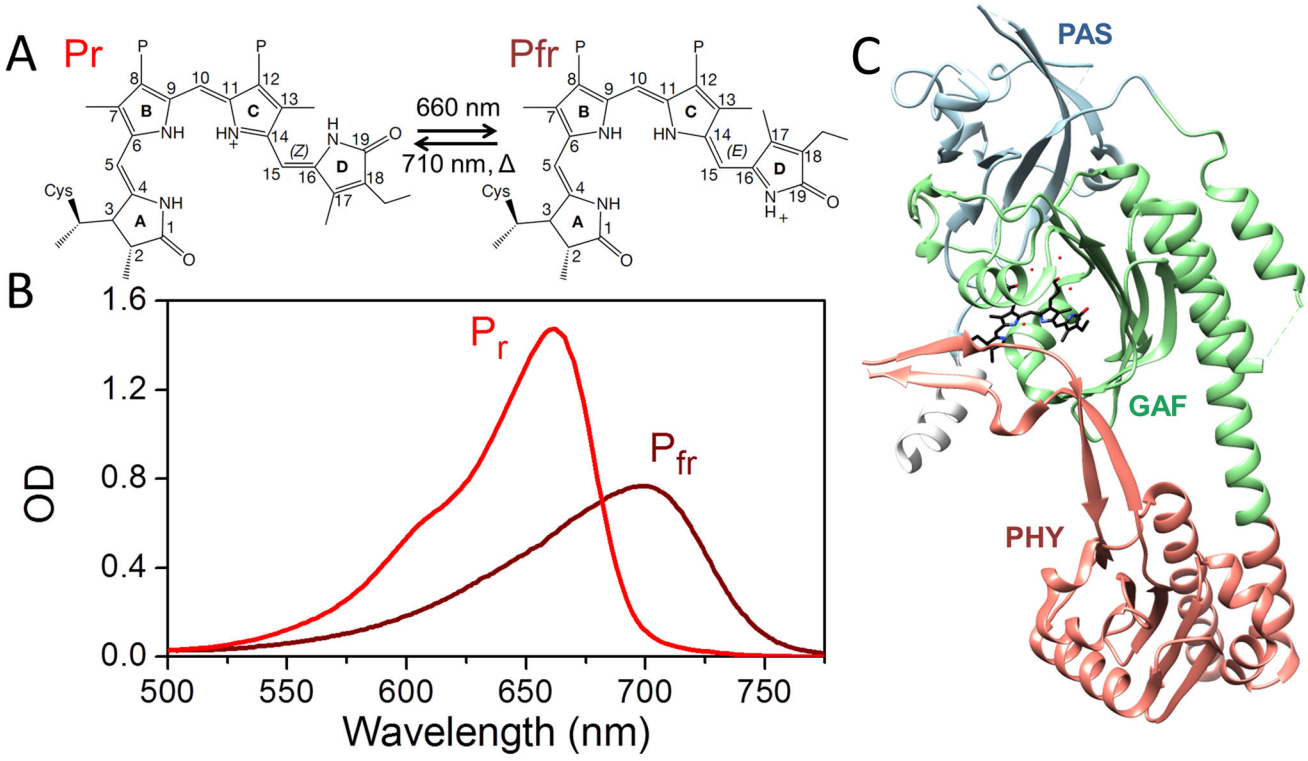

Figure 1.

(A) The phycocyanobilin (PCB) chromophore of Cph1 is shown in the *15Z* (right) and *15E* (left) conformations. (B) Absorption spectra are shown for dark-adapted P_r with a *15Z* PCB chromophore (red) and for calculated P_{fr} with a *15E* PCB chromophore (dark red) at pH 8.[52] (C) The crystal structure showing PAS-GAF-PHY domain architecture of Cph1.[15]

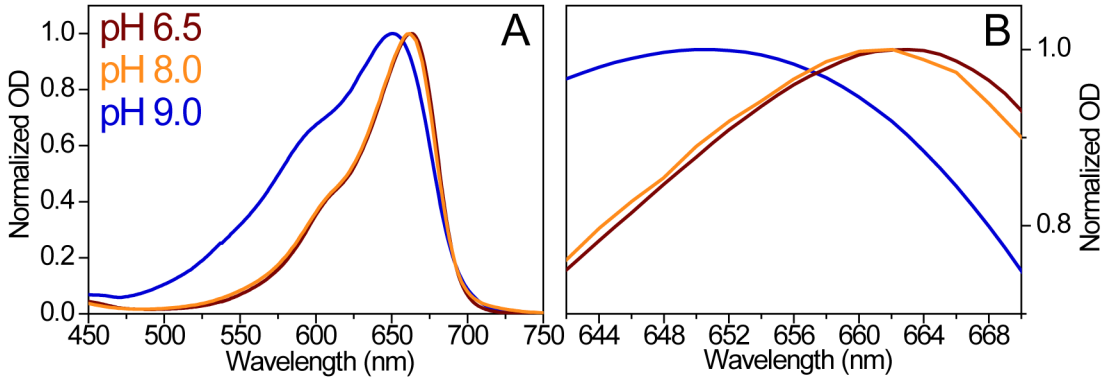

Figure 2.

(A) Normalized static absorption spectra are shown for Cph1Δ in the P_r state at pH 6.5 (dark red curve), pH 8.0 (orange curve) and pH 9.0 (blue curve). (B) Detailed view of the peak region.

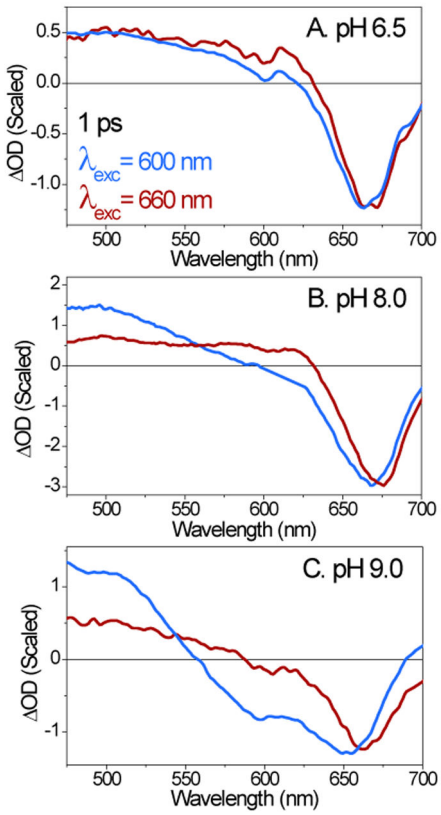

Figure 3.

Comparison of the DEWI TA spectra of Cph1Δ 1 ps after excitation at 600 nm (blue curves) and 660 nm (red curves) at pH 6.5 (A), pH 8.0 (B) and pH 9.0 (C). The spectra obtained at 600 nm excitation are scaled to the amplitude of the band at 660–675 nm of the spectra obtained at 660 nm excitation at pH 8.0. DEWI spectra at 0.5 ps and 5 ps are presented in Figs. S1 and S2.

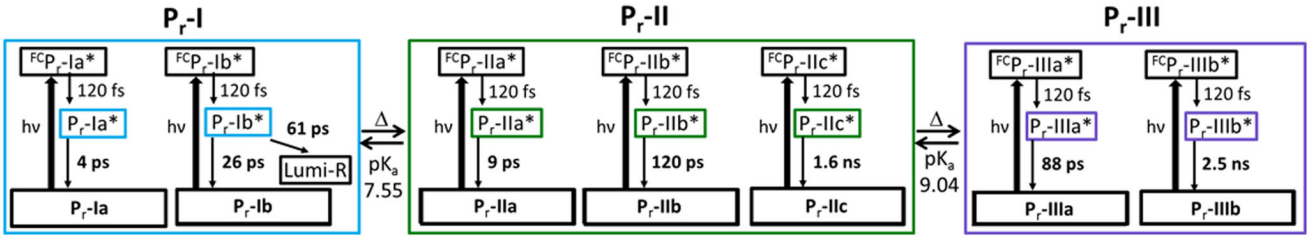

Figure 4.

Integrated target model for DEWI TA signals at different pH values (6.5, 8.0, and 9.0). P_r populations P_r-I, P_r-II, and P_r-III are colored teal, green, and purple, respectively. The relative occupancies of initially excited populations under different experimental conditions are shown in Table S1. The pKa values are estimated from Escobar et al.[36]

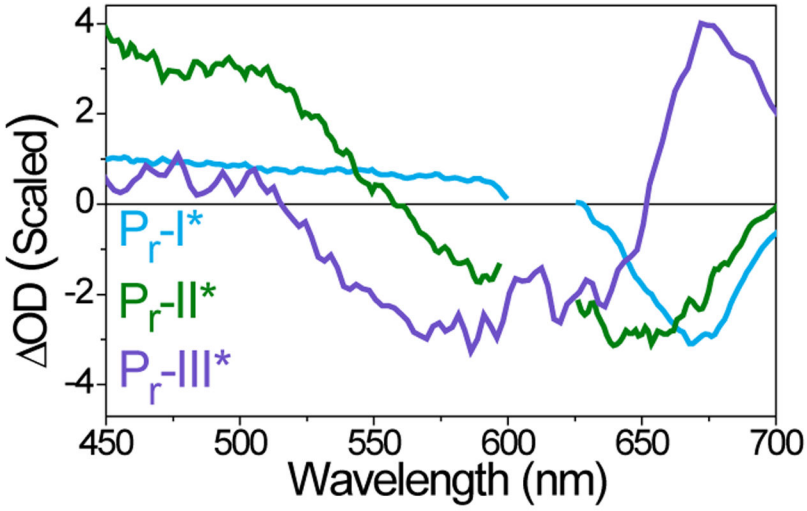

Figure 5.

Comparison of SADS for different excited-state P_r populations: photoactive (P_r-I*, teal curve), fluorescent (P_r-II*, green curve) and deprotonated (P_r-III*, purple curve). The model is summarized in Fig. 4 with parameters in Table S1.

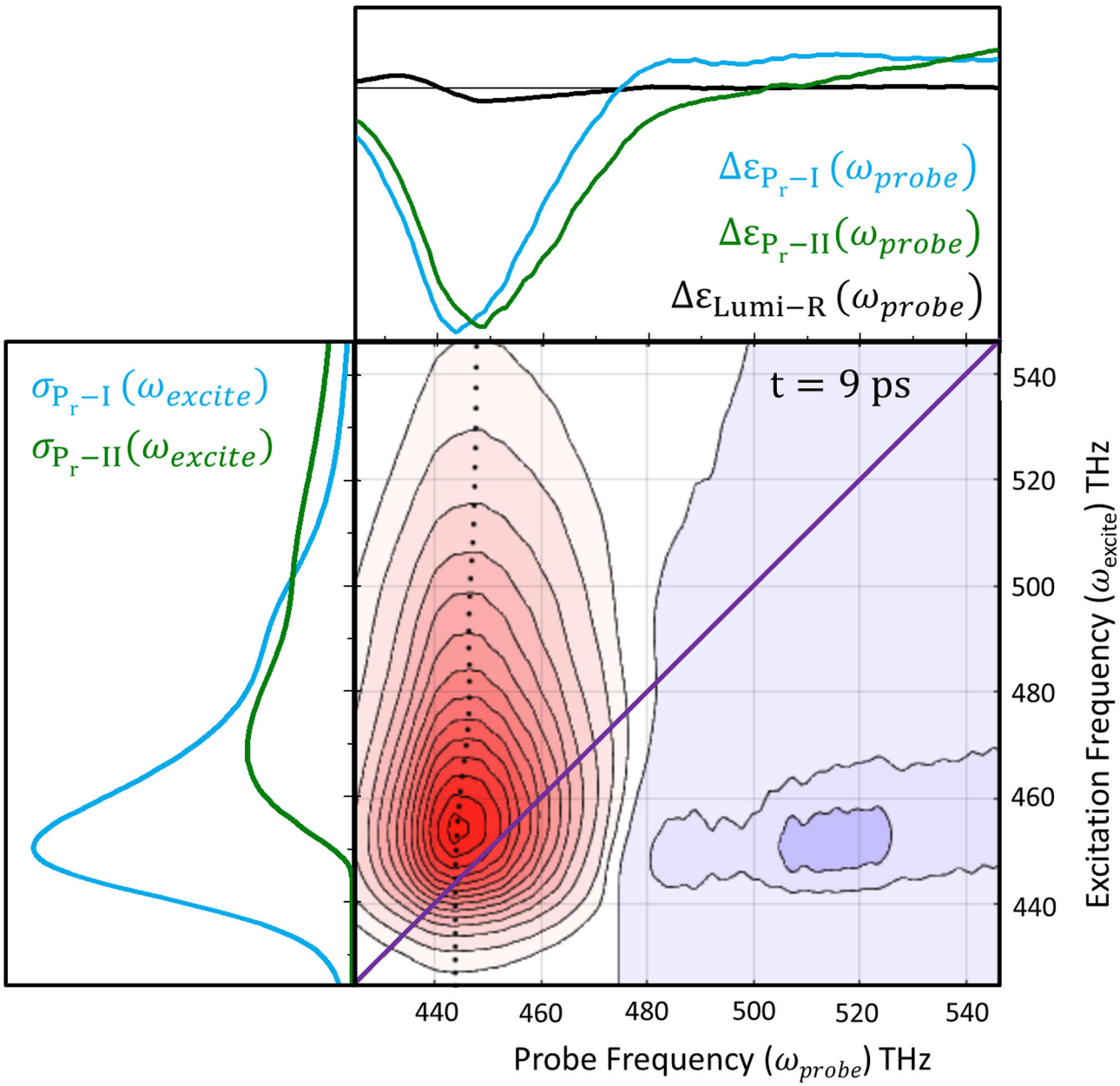

Figure 6.

Simulated 2D electronic spectrum at 9 ps calculated using the model proposed in Figs. 4 and 5 with parameters in Table S1. Purple line, the diagonal; filled circles, peak of the bleach/SE band as a function of excitation frequency. The absorption spectra (left curves) and SADS (top curves) are color coded to match the P_r-I and P_r-II populations in the global model of Fig. 4.

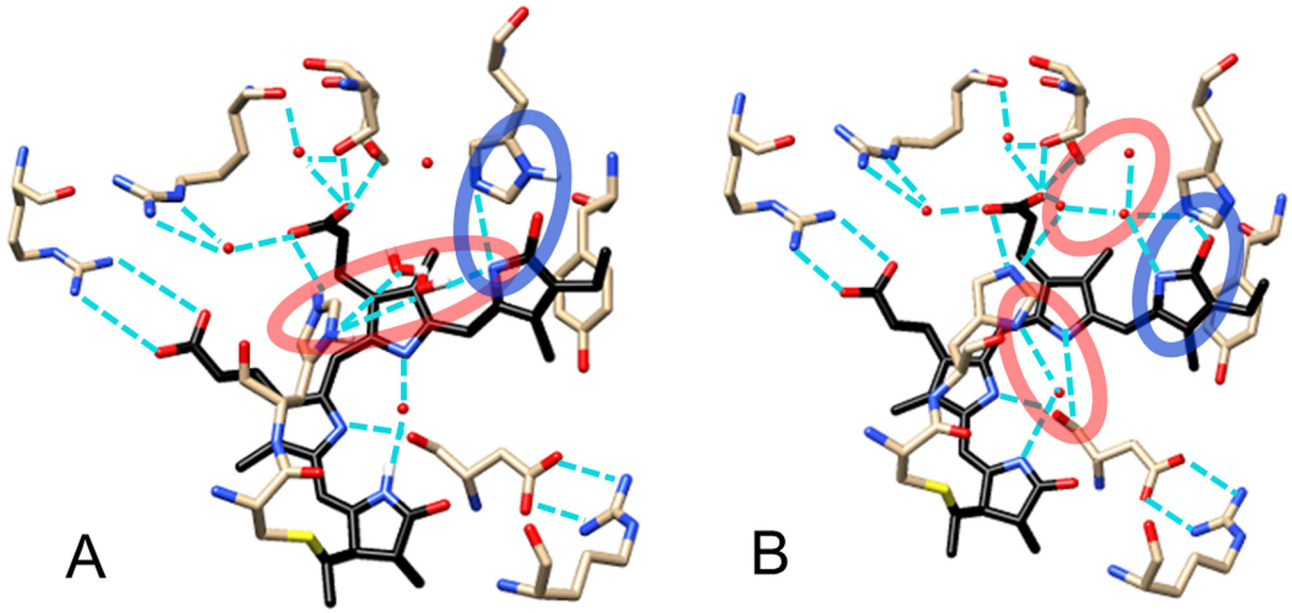

Figure 7.

Chromophore pocket of Cph1 in the proposed P_r-I and P_r–II configurations.[15, 46] (A) Model of the proposed hydrogen bonding network (teal dashed lines) formed when His260 is protonated, derived from solid-state NMR and resonance Raman spectroscopy.[46] (B) P_r-II crystal structure (2VEA).[15] Alternative perspectives are shown in Figs. S8 and S9.